# *rp* Process and Masses of $N \approx Z \approx 34$ Nuclides

J. Savory,* P. Schury, C. Bachelet, M. Block, G. Bollen, M. Facina, C. M. Folden III, C. Guénaut, E. Kwan, A. A. Kwiatkowski, D. J. Morrissey, G. K. Pang, A. Prinke, R. Ringle, H. Schatz, S. Schwarz, and C. S. Sumithrarachchi

*National Superconducting Cyclotron Laboratory, Michigan State University, East Lansing, Michigan 48824, USA*

(Received 10 October 2008; published 30 March 2009)

High-precision Penning-trap mass measurements of the $N \approx Z \approx 34$ nuclides $^{68}$Se, $^{70}$Se, $^{70m}$Br, and $^{71}$Br were performed, reaching experimental uncertainties of 0.5–15 keV. The new and improved mass data together with theoretical Coulomb displacement energies were used as input for *rp* process network calculations. An increase in the effective lifetime of the waiting point nucleus $^{68}$Se was found, and more precise information was obtained on the luminosity during a type I x-ray burst along with the final elemental abundances after the burst.

DOI: 10.1103/PhysRevLett.102.132501 PACS numbers: 21.10.Dr, 26.30.−k, 27.50.+e

Type I x-ray bursts can occur when a neutron star accretes matter from an expanded companion star. In order to understand the energy generation, the fuel consumption, and the ash composition of type I x-ray bursts the underlying nuclear physics must be known. Masses of the nuclides involved in this process are critical to the understanding of these events [1].

Type I x-ray bursts are initiated when the temperature and the density in the accreted layer on a neutron star become high enough to allow a breakout from the hot CNO cycle. The burst consists of a rapid burning of hydrogen in a series of proton captures and $\beta$ decays, a scenario generally known as the *rp* process [2]. The nuclei start to capture protons and proceed along a capture chain until the proton dripline is reached. The burst can only proceed past this point through a $\beta$ decay or a double proton capture. These dripline nuclei are known as the ''waiting points.'' The time it takes to proceed beyond a waiting point nucleus, the effective lifetime, determines the extent to which the waiting point alters the final abundance distribution and the observable x-ray light curve of the burst.

The important waiting point nuclei in the $N \approx Z \approx 34$ region are $^{64}$Ge, $^{68}$Se, and $^{72}$Kr. These nuclei along with an *rp* process path in this region are shown in Fig. 1. Their effective lifetimes have a strong impact on the shape and the duration of the light curve emitted during a type I x-ray burst [3–6]. In particular, their long lifetimes are a likely explanation for the often observed long burst tails, which are commonly used as indicators of a hydrogen content sufficient to sustain an extended *rp* process beyond $A = 64$. A quantitative interpretation of burst tails in terms of the initial hydrogen content requires reliable nuclear physics. Such a quantitative analysis is not only a precision test of burst models but also allows for a determination of the expected maximum luminosity (Eddington luminosity) that is observed in powerful photospheric radius expansion bursts. A quantitative understanding of photospheric radius expansion bursts could pave the way for using them as standard candles [7] or as probes of the nuclear matter equation of state [8]. A reliable modeling of burst tails is also important to predict the composition of the burst ashes. This composition is required to perform crust model calculations [9] and to predict possible contributions to galactic nucleosynthesis from small amounts of matter ejected in some bursts [10].

The effective lifetime of a waiting point depends very sensitively on nuclear masses. During the explosion, an equilibrium develops between proton capture and photodisintegration. The ratio of the rates determines the extent to which the double proton capture channel can bypass the $\beta$ decay of the waiting point nuclei. Reliable rate ratio calculations require mass measurements with uncertainties on the order of 10 keV or less [1,3]. Because of the low production rates of nuclides close to the proton dripline in laboratory nuclear reactions, mass measurements in this region are difficult. However, recent progress in Penning-trap mass spectrometry [11] has allowed many of the masses up to the $N \approx Z \approx 34$ region to be measured with high precision [12–17].

In this Letter, we present high-precision Penning-trap mass measurements of $^{68}$Se, $^{70}$Se, $^{70m}$Br, and $^{71}$Br. This set of precise experimental mass data provides a solid basis for predicting mass values beyond the $N = Z$ line using Coulomb displacement energies (CDE), the binding energy difference between the mirror nuclei, calculated in [6]. The improved mass data and predictions were used as

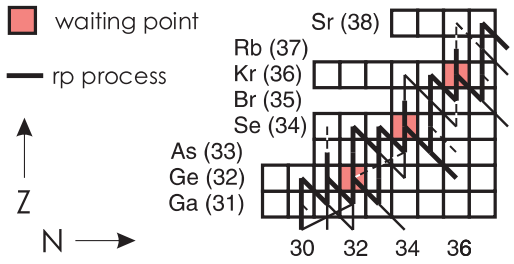


FIG. 1 (color online). Proposed path of the *rp* process in the $N \approx Z \approx 34$ region and waiting point nuclei.

 

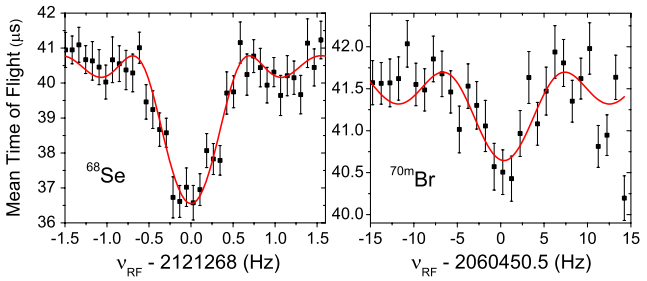


FIG. 2 (color online). Cyclotron resonances obtained for $^{68}$Se and $^{70m}$Br. Excitation times of $T_{RF} = 1.25$ s and 100 ms were used, leading to resolving powers of $R \approx 3\,000\,000$ and 300 000, for $^{68}$Se and $^{70m}$Br, respectively.

input for an $rp$ process network calculation, allowing for more reliable modeling of x-ray burst tails.

The experiment was performed with the Low Energy Beam and Ion Trap (LEBIT) facility [18] installed at the Coupled Cyclotron Facility of the National Superconducting Cyclotron Laboratory (NSCL). Its main components are a gas cell [19], a radio frequency quadrupole ion guide system [14], a beam cooler and buncher [20], and a high-precision Penning trap located in the center of a $B = 9.4$ T superconducting solenoid. LEBIT is at present the only facility for Penning-trap mass measurements of rare isotopes produced by projectile fragmentation [14,18,21,22]; thus, LEBIT can access isotopes difficult to obtain with other techniques.

The nuclides $^{68}$Se, $^{70}$Se, $^{70m}$Br, and $^{71}$Br studied in this work were produced by projectile fragmentation of a 150 MeV/$u$ primary $^{78}$Kr beam and in-flight separated by the NSCL's A1900 separator [23]. The ions of interest are stopped and thermalized in the gas cell [19]. The selenium ions were extracted from the gas cell as singly charged atomic ions. The bromine ions were predominantly extracted in the form of atomic $^{70m}Br^+$ and molecular $^{71}BrH_2^+$. The beam was purified and transported to the Penning trap using techniques and components discussed in [24]. Once in the high-precision Penning trap the mass $m$ of the ion with charge $q$ was determined through a measurement of its cyclotron frequency, $\omega_c = qB/m$, using a time-of-flight resonance detection technique [25,26]. Results of a typical resonance curve are shown in Fig. 2. For the measurements of $^{68}$Se, $^{70m}$Br, and $^{71}BrH_2$ the number of ions detected on a microchannel plate detector after the trap (assuming a detection efficiency of 30%) was on average kept below one ion per trap cycle. This was done to minimize systematic effects due to the interaction of simultaneously stored ions with different masses [27].

Each measurement of the cyclotron frequency of a rare isotope $\omega_c$ was bracketed with that of a stable reference ion $\omega_{c,\mathrm{ref}}$ with a well-known mass extracted from the gas cell. At least four individual measurements were performed per isotope. Table I summarizes the nuclides studied in this work together with the reference ions used and the average of obtained cyclotron frequency ratios $R = \omega_c/\omega_{c,\mathrm{ref}}$. The uncertainties given are purely statistical except for the measurement of $^{70}$Se. In this case on average about six ions were stored in the trap. These measurements were analyzed for possible systematic frequency shifts due to the simultaneous storage of undesired ions [27]. A small relative shift of $1.6 \times 10^{-8}$ was found and a corresponding correction was applied to the final result. Additional possible systematic effects due to relativistic mass shifts or residual trapping field imperfections were considered but not taken into account since they are well below the quoted uncertainties.

TABLE I. Nuclides investigated together with the half-life ($T_{1/2}$), the reference ion used (Ref.), the number of individual cyclotron frequency measurements ($N$), and the averaged frequency ratio $\bar{R}$.

| | $T_{1/2}$ | Ref. | $N$ | $\bar{R}$ |
|---|---|---|---|---|
| $^{68}$Se | 35.5 s | $^{12}C^{19}F_3$ | 12 | 1.015 504 334(8) |
| $^{70}$Se | 41.1 m | $^{13}C^{19}F_3$ | 4 | 1.000 930 159(24) |
| $^{70m}$Br | 2.2 s | $^{13}C^{19}F_3$ | 7 | 1.000 733 57(23) |
| $^{71}BrH_2$ | 21.4 s | $^{12}C_4H_9{}^{16}O$ | 4 | 1.001 512 556(80) |

The mass values of the rare isotopes were determined using the obtained frequency ratio and the reference ion mass [28], the results are shown in Table II. The mass values from the 2003 Atomic Mass Evaluation (AME'03) [28] and their difference with the LEBIT data are also listed. The table also presents mass values for $^{70}$Kr and $^{71}$Kr. These are predictions obtained from the experimental mass values for $^{70}$Se and $^{71}$Br together with the calculated CDE of 22 190(100) and 11 260(100) keV, respectively [6].

The mass uncertainties obtained range from 500 eV for $^{68}$Se to about 15 keV for $^{70m}$Br. This constitutes an improvement in precision by factors of 40 and more. The new mass values, shown in Fig. 3, are in good agreement with those listed in AME'03 [28] except $^{70}$Se. Results from time-of-flight measurements from [29,30] of $^{70}$Se agree with the more precise LEBIT value. Deviations of more than $2\sigma$ are observed for results from a $\beta^+$ decay [31] and a storage ring time-of-flight measurement [32]. Of the isotopes studied only $^{68}$Se was measured in a Penning

TABLE II. Mass excess values (ME) in keV obtained with LEBIT, from AME'03 [28] and the difference $\Delta\mathrm{ME} = \mathrm{ME}_{\mathrm{AME'03}} - \mathrm{ME}_{\mathrm{LEBIT}}$. Also given are new mass predictions for $^{70}$Kr and $^{71}$Kr.

| Species | $\mathrm{ME}_{\mathrm{LEBIT}}$ | $\mathrm{ME}_{\mathrm{AME'03}}$ | $\Delta$ME |
|---|---|---|---|
| $^{68}$Se | −54 189.3(5) | −54 210(30) | −21(30) |
| $^{70}$Se | −61 929.7(1.6) | −62 050(60) | −120(60) |
| $^{70}$Br | −51 425(15) | −51 430(310) | −5(310) |
| $^{71}$Br | −56 502.4(5.4) | −57 060(570) | −558(570) |
| | $\mathrm{ME}_{\mathrm{LEBIT+CDE}}$ | $\mathrm{ME}_{\mathrm{AME'03}}$ | $\Delta$ME |
| $^{70}$Kr | −41 304(100) | −41 680(390) | −376(403) |
| $^{71}$Kr | −46 025(100) | −46 920(650) | 895(658) |

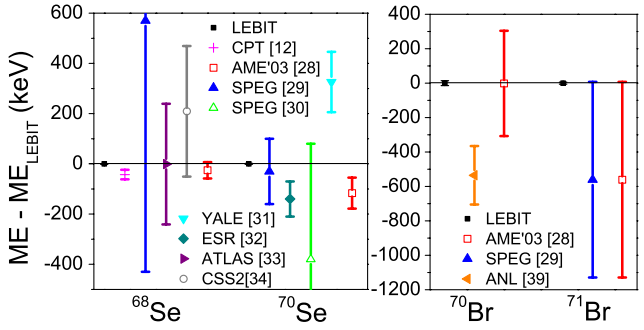


FIG. 3 (color online). A comparison between the LEBIT mass values and from previous experiments [12,29–34,39] and AME'03 [28].

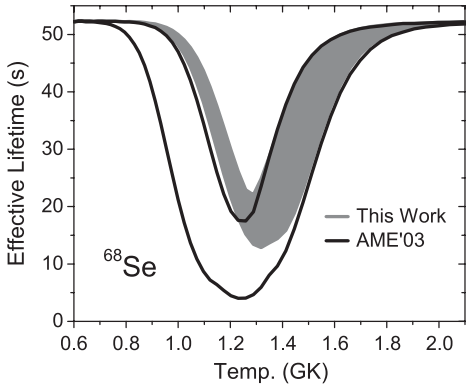


FIG. 4. Effective lifetime versus temperature obtained from a local *rp* process calculation using the data from this work and compared to using values from AME'03 [28] and CPT [12].

trap previously. The Canadian Penning-trap (CPT) mass value [12] disagrees by $\approx 2\sigma$ with the more precise LEBIT result. Mass values of $^{68}$Se have also been obtained from $\beta^+$ decay [33] and time-of-flight [29,34,35] measurements. While data from [29,33,34] agree with our value, the result given in [35] shows a $23\sigma$ deviation and thus was not included in Fig. 3.

The proton dripline nuclide $^{70}$Br has a $J^\pi = 0^+$ ground state with a half-life of $T_{1/2} = 79.1(8)$ ms lifetime and a longer-lived, $T_{1/2} = 2.2(2)$ s, $J^\pi = 9^+$ $\beta$-decaying isomeric state [36,37] with an excitation energy of 2292.2 (8) keV [38]. Considering that the half-lives of the two states and the time the ions spend in the apparatus is more than 200 ms before detection, we concluded that the measured resonance corresponds to that of the longer-lived isomeric state. Hence, the ground state mass value given in Table II was calculated using the known excitation energy and the measured mass value for the excited state. A preliminary mass value for $^{70}$Br was given in [39], but excluded since 1993 from the AME [40] due to a conflict with the mass systematic trends in this region. Our measurement disagrees with [39] by 535 keV and thus supports this rejection.

The precise mass values obtained in this and earlier LEBIT work [14] together with the use of CDE [6] significantly improved $Q$ values near $^{64}$Ge and $^{68}$Se. With these $Q$ values and $(p, \gamma)$ reaction rates from [41], the reverse $(\gamma, p)$ reaction rates were calculated using detailed balance [5]. For part of this analysis all $Q$ values in the $N \approx Z \approx 34$ region were varied within their uncertainties in order to determine the mass uncertainties in the reverse reaction rates. *rp* process network calculations were then performed using the new reverse reaction rates in the $N \approx Z \approx 34$ region and reaction rates from [41] everywhere else.

A local network calculation, similar to that used previously for $^{64}$Ge [14], was employed to determine the effective lifetime of $^{68}$Se as a function of temperature, and the result is shown in Fig. 4. The previous effective lifetime of 10.7(6.8) s (which includes the CPT mass value for $^{68}$Se [12]) still allowed within error bars for the possibility of a lifetime on the order of a few seconds. For such lifetimes, much shorter than typical burst time scales of 10–100 s, $^{68}$Se would not be a strong waiting point anymore. With the new lifetime of 17.4(4.5) s it is now clear that $^{68}$Se is a strong waiting point for all prevalent conditions. This is mostly due to our new measurement of the $^{70}$Se mass and the $^{69}$Se LEBIT mass measurement reported in [14] that allowed us to improve the mass predictions for $^{70}$Kr and $^{69}$Br using CDE [6].

With our measurement all masses needed to constrain the effective lifetimes of the major *rp* process waiting points $^{64}$Ge, $^{68}$Se, and $^{72}$Kr, with the help of theoretical CDE, are now known. These are the masses of $^{64-66}$Ge, $^{68-70}$Se, and $^{72-74}$Kr. In order to determine the effects of the improved proton capture $Q$ values on the x-ray light curve and the final element abundances of a type I x-ray burst, a full network calculation was performed using a single-zone burst model [5] as an example. The x-ray luminosity as a function of time, the light curve, is the main direct experimental observable of a type I x-ray burst. Figure 5 shows the light curves of a burst calculated with different sets of mass data. The envelope shows the variation in luminosity and time caused by the corresponding mass uncertainties in the $N \approx Z \approx 34$ region. The light curve obtained with the LEBIT data has considerably smaller uncertainty and reveals a reduced time scale of the burst. The remaining mass uncertainties in the light curve are mainly due to a few still unmeasured masses, e.g., $^{65}$As, $^{69}$Br, and $^{73}$Rb, which are beyond the $N = Z$ line and in some cases the nuclei ($^{69}$Br, $^{73}$Rb) are thought to be proton unbound.

Clearly, with our mass measurement being the latest step, a significant improvement in the nuclear physics input for x-ray bursts has now been achieved. This will allow for a more reliable simulation of extended burst tails and it opens the door for a quantitative analysis of x-ray burst models and extraction of system parameters. To compare with specific x-ray bursts will require a model that accurately simulates the radiation transport to the surface, and

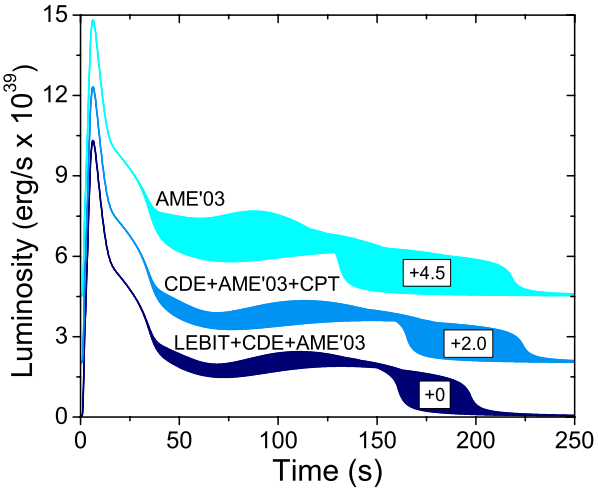


FIG. 5 (color online). X-ray luminosity as a function of time using the AME'03 [28], the AME'03 including a measurement of $^{68}$Se from [12] and CDE from [6], and the data presented in this work for $Q$ values in the $N \approx Z \approx 34$ region. For clarity the different curves were offset by the amount shown in boxes.

simulations for a range of accretion rates, accreted compositions, and neutron star properties.

The overall impedance of the $rp$ process reaction flow by the waiting points in the $A = 64$–$72$ mass region strongly affects the production of heavier nuclei in the burst ashes. The final $rp$ process abundances from our model are shown in Fig. 6. The longer lifetime of $^{68}$Se found in this work increases the amount of $A = 68$ nuclei. The more reliable effective lifetimes of the $A = 64$–$72$ reduce the uncertainty in the production of heavier nuclei in the $rp$ process introduced by this major bottleneck. Our improved nuclear masses are therefore an important step towards a reliable estimate of the composition of the ashes of x-ray bursts needed to model neutron star crust processes and to predict signatures of small amounts of ejected material.

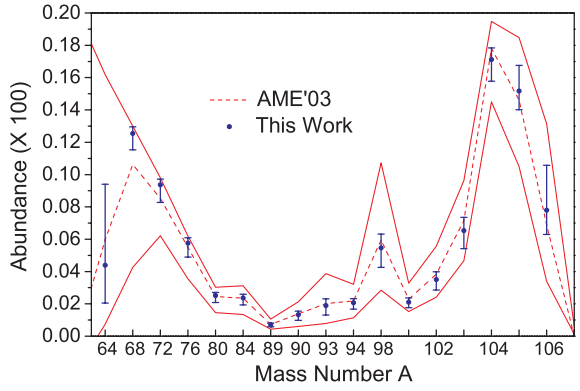


FIG. 6 (color online). Final element abundance from a type I x-ray burst obtained using the LEBIT data set and from the AME'03 [28] including a measurement of $^{68}$Se from [12] for $Q$ values in the $N \approx Z \approx 34$ region.

We wish to acknowledge the support of Michigan State University, the National Science Foundation Grant No. PHY-06-06007, and the U.S. Department of Energy Contract No. DE-FG02-00ER41144. H. S. acknowledges support from NSF Grant No. PHY 02-16783 (Joint Institute for Nuclear Astrophysics).

*savory@nscl.msu.edu

[1] H. Schatz, Int. J. Mass Spectrom. **251**, 293 (2006).
[2] R. Wallace and S. Woosley, Astrophys. J. Suppl. Ser. **45**, 389 (1981).
[3] O. Koike *et al.*, Astron. Astrophys. **342**, 464 (1999).
[4] H. Schatz *et al.*, Phys. Rev. Lett. **86**, 3471 (2001).
[5] H. Schatz *et al.*, Phys. Rep. **294**, 167 (1998).
[6] B. A. Brown *et al.*, Phys. Rev. C **65**, 045802 (2002).
[7] D. K. Galloway *et al.*, Astrophys. J. **639**, 1033 (2006).
[8] F. Ozel, Nature (London) **441**, 1115 (2006).
[9] S. Gupta *et al.*, Astrophys. J. **662**, 1188 (2007).
[10] N. N. Weinberg *et al.*, Astrophys. J. **639**, 1018 (2006).
[11] K. Blaum, Phys. Rep. **425**, 1 (2006).
[12] J. A. Clark *et al.*, Phys. Rev. Lett. **92**, 192501 (2004).
[13] J. A. Clark *et al.*, Phys. Rev. C **75**, 032801(R) (2007).
[14] P. Schury *et al.*, Phys. Rev. C **75**, 055801 (2007).
[15] C. Guénaut *et al.*, Phys. Rev. C **75**, 044303 (2007).
[16] D. Rodríguez *et al.*, Phys. Rev. Lett. **93**, 161104 (2004).
[17] T. Eronen *et al.*, Phys. Lett. B **636**, 191 (2006).
[18] G. Bollen *et al.*, Phys. Rev. Lett. **96**, 152501 (2006).
[19] L. Weissman *et al.*, Nucl. Phys. **A746**, 655 (2004).
[20] S. Schwarz *et al.*, Nucl. Instrum. Methods Phys. Res., Sect. B **204**, 474 (2003).
[21] R. Ringle *et al.*, Phys. Rev. C **75**, 055503 (2007).
[22] M. Block *et al.*, Phys. Rev. Lett. **100**, 132501 (2008).
[23] D. J. Morrissey *et al.*, Nucl. Instrum. Methods Phys. Res., Sect. B **204**, 90 (2003).
[24] P. Schury *et al.*, Hyperfine Interact. **173**, 165 (2006).
[25] G. Bollen *et al.*, J. Appl. Phys. **68**, 4355 (1990).
[26] M. König *et al.*, Int. J. Mass Spectrom. Ion Processes **142**, 95 (1995).
[27] G. Bollen *et al.*, Phys. Rev. C **46**, R2140 (1992).
[28] G. Audi, A. Wapstra, and C. Thibault, Nucl. Phys. **A729**, 337 (2003).
[29] G. F. Lima *et al.*, Phys. Rev. C **65**, 044618 (2002).
[30] M. Chartier *et al.*, Nucl. Phys. **A637**, 3 (1998).
[31] B. E. Tomlin *et al.*, Phys. Rev. C **63**, 034314 (2001).
[32] M. Hausmann *et al.*, Hyperfine Interact. **132**, 289 (2001).
[33] A. Wöhr *et al.*, Nucl. Phys. **A742**, 349 (2004).
[34] M. B. Gómez-Hornillos *et al.*, Phys. Rev. C **78**, 014311 (2008).
[35] A. S. Lalleman *et al.*, Hyperfine Interact. **132**, 313 (2001).
[36] A. Piechaczek *et al.*, Phys. Rev. C **62**, 054317 (2000).
[37] Vosicki *et al.*, Nucl. Instrum. Methods **186**, 307 (1981).
[38] D. G. Jenkins *et al.*, Phys. Rev. C **65**, 064307 (2002).
[39] C. Davids, in *Proceedings of the Sixth International Conference on Atomic Masses, East Lansing, MI, 1979* (Plenum, New York, 1980), p. 419.
[40] G. Audi and A. Wapstra, Nucl. Phys. **A565**, 1 (1993).
[41] T. Rauscher and F.-K. Thielemann, At. Data Nucl. Data Tables **75**, 1 (2000).